

Imaging of single infrared, optical, and ultraviolet photons using distributed tunnel junction readout on superconducting absorbers

Miha Furlan, Eugenie Kirk, and Alex Zehnder

Laboratory for Astrophysics, Paul Scherrer Institute, 5232 Villigen PSI, Switzerland

(Dated: July 11, 2018)

Single-photon imaging spectrometers of high quantum efficiency in the infrared to ultraviolet wavelength range, with good timing resolution and with a vanishing dark count rate are on top of the wish list in earth-bound astronomy, material and medical sciences, or quantum information technologies. We review and present improved operation of a cryogenic detector system potentially offering all these qualities. It is based on a superconducting absorber strip read out with superconducting tunnel junctions. The detector performance is discussed in terms of responsivity, noise properties, energy and position resolution. Dynamic processes involved in the signal creation and detection are investigated for a basic understanding of the physics, and for possible application-specific modifications of device characteristics.

PACS numbers: 07.60.Rd, 42.79.Pw, 85.25.Oj

I. INTRODUCTION

Superconducting tunnel junction (STJ) detectors are among the most advanced cryogenic sensors¹ with intrinsic spectroscopic resolution and high detection efficiency over a broad energy range. Essential advantages of low-temperature detectors in general are the small energy gap in superconductors compared to standard semiconductors (typically three orders of magnitude lower), decoupling of the electron and phonon systems in normal metals below about 50 mK, and a vanishing lattice heat capacity.

The lifetime of nonequilibrium quasiparticles generated in superconductors due to local energy deposition in excess of a purely thermal distribution becomes very large at operating temperatures well below the transition temperature. Those quasiparticles can be efficiently detected as a tunnel current in an STJ if tunneling rates are high compared to recombination and loss processes. In the tunneling process, a quasiparticle can tunnel back and contribute many times to the total charge transfer.² This internal amplification process is a unique feature of STJs which significantly improves the sensitivity of the detectors, allowing us to observe single sub-eV energy quanta.

As a next generation detector, STJs are very promising candidates e.g. for astronomical observations.^{3,4} In addition to their direct spectroscopic response and high speed ($\lesssim 10^5$ counts/s), they can be operated with essentially no dark count rate, which is another enormous advantage compared to CCD imaging systems, making them the favored choice for detection of faint objects. However, to satisfy the desire for detectors with imaging capabilities as offered by CCD cameras, a competitive STJ based multipixel camera inevitably faces the complexity of large channel-number readout, i.e. the problem of transferring the small charge-signals from the cryogenic environment to external room-temperature electronics. One possible solution to reduce the number of readout lines is by using distributed readout imaging de-

vices (DROIDs), where the quasiparticle distribution in a large superconducting absorber is detected with several STJs at different positions. This type of detector was investigated with x-rays^{5,6,7,8,9,10,11} as well as with optical photons.^{12,13,14,15,16}

In this paper we present measurements with quasi-one-dimensional DROIDs irradiated with energy quanta covering the ultraviolet (UV) and the entire optical range, and including an extension to near infrared (IR) energies below 1 eV. After a description of device properties, experimental conditions and measurement procedure in Sec. II, the linearity of detector response, the noise performance and the resolution in energy and position are discussed in Sec. III A. Time-dependent processes in the detector involving quasiparticle diffusion, loss and trapping rates, are considered in more detail in Sec. III B. The paper concludes in Sec. IV.

II. EXPERIMENT

The devices were fabricated by sputter deposition on a sapphire substrate. The Ta absorber was deposited first, with an area of $L_{\text{Ta}} \times W_{\text{Ta}} = 135 \times 31.5 \mu\text{m}^2$ and a thickness of 100 nm. The square shaped Ta-Al junctions with a side length $L_j = 25 \mu\text{m}$ and an Al layer thickness of 38 nm were fabricated at each end on top of the absorber. Hence, the length of the bare absorber was $L_{\text{b,Ta}} = 80 \mu\text{m}$. The residual resistivity ratio of the absorber was $RRR = \rho_{\text{RT}}/\rho_{\text{LT}} \approx 25$, where ρ_{RT} and ρ_{LT} are the (normal) resistivities at room temperature and low temperature, respectively.

The cryogenic detectors were operated at 310 mK and the supercurrent was suppressed by application of a magnetic field parallel to the tunnel barrier. With two independent charge-sensitive preamplifiers operated at room temperature the devices were voltage biased at $V_b = 80 \mu\text{V}$ where a thermal current below 50 pA was measured. At this bias voltage the current I was found to depend on temperature T according to the empirical

expression $I = 0.345 \exp(T/26.4 \text{ mK}) \text{ fA}$. Although the minimum thermal current was observed at $V_b \approx 200 \mu\text{V}$, the responsivity of the devices showed a maximum at lower V_b , in the range of negative differential resistance of the current-voltage characteristics. We introduced ohmic resistors of $5 \text{ k}\Omega$ in the signal lines (in series) close to the devices, which acted together with the junction capacitances as efficient RC filters against high-frequency noise on the 1.2 m cables, as well as damping resistors against resonances of the junction-cable system corresponding to an LRC circuit with intrinsically low damping constant. Compared to the superconducting device resistance on the order of $1 \text{ M}\Omega$ the influence of the filters on the detector response was negligible.

A variety of pulsed light-emitting diodes (LEDs) was used as light sources, with wavelengths ranging from IR at 1550 nm (0.801 eV) to UV at 370 nm (3.355 eV). The specified spectral widths of the LEDs were typically a few percent. The photons were coupled to the detectors via optical fibres and through the sapphire substrate. Back-illumination through the substrate was found to be essential for optimum detector performance, probably thanks to a clean, oxide-free interface, whereas the native TaO_x on top of the absorber appears to be less transparent. The light intensity (pulse duration) was adjusted to observe on the order of one photon per pulse. Packets of (incoherent) multiple photons were synchronized to a maximum time spread of less than 200 ns .

Detection efficiency of Ta absorbers is about 60% for optical and UV photons, but it drops drastically below red photon energies $\lesssim 2 \text{ eV}$.¹⁷ Radiation shorter than about 200 nm is expected to be cut off by the sapphire substrate.¹⁸ Unfortunately, we had no reference system for calibrating the absolute photon absorption probability.

The electronic signals from the preamplifiers had a rise-time of about $1 \mu\text{s}$ (comparable to the tunneling time and to the $\sim 1 \text{ MHz}$ bandwidth of the readout electronics) and a decay on the order of $30 \mu\text{s}$. The preamplifier outputs were band-pass filtered with a $10 \mu\text{s}$ time constant and digitized for offline analysis.

Due to noticeable dependence of the device responsivity on V_b and on electronics settings the system was calibrated against an electronic pulser injecting a defined number of charges. The charge noise of the readout electronics with the junctions connected (but not irradiated) was determined from pulser distribution spread or from rms noise measurements to be $q_e \approx 2760 \text{ e}$ for both channels combined, i.e. about 1950 e for each individual channel (at $V_b = 80 \mu\text{V}$).

Figure 1 shows results from measurements with UV as well as with IR photons. The charges Q_1 and Q_2 refer to the separate outputs from the two channels. The left-hand plots display the total charge $Q_\Sigma = Q_1 + Q_2$ versus the normalized (onedimensional) position of the photon interaction $x_0 = (Q_1 - Q_2)/Q_\Sigma$. Slight asymmetries of the data with respect to x_0 are due to the difficulty of perfect adjustment of operating point for the two chan-

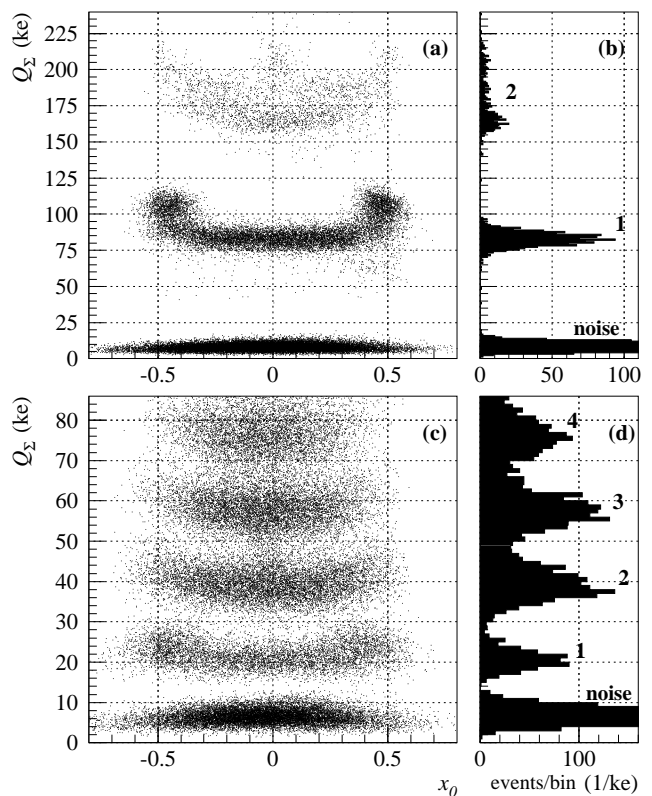


FIG. 1: (a) Total charge output Q_Σ versus normalized position for the DROID irradiated with 3.355 eV (370 nm) UV photons. (b) Projection of the charge spectrum (histogram) of the data in (a) for $|x_0| < 0.05$. The labels to the right of the peaks refer to the number of simultaneous photons, noise-triggered events are labelled with ‘noise’. (c),(d) Data as presented in (a),(b), but with the detector irradiated with 0.801 eV (1550 nm) IR photons.

nels. The shape of the event distribution is determined (in first order) by quasiparticle diffusion, loss processes, local energy gap, and the efficiencies of trapping and tunneling (see Sec. III B).

Spectral response and resolution of the experimental data are determined for events with $|x_0| < 0.05$, a projection of which is shown in the right-hand plots of Fig. 1. The number of simultaneously absorbed energy quanta is given to the right of the corresponding peaks, whereas ‘noise’ denotes events triggered on photonless fluctuations. A clear spectral separation of single-photon events from multiple photons and from noise triggers is observed, down to the lowest measured IR energy quanta of 0.801 eV

III. DISCUSSION

As a first remark, we wish to comment on the events observed in Fig. 1(a) in the range ($0.3 \lesssim x_0 \lesssim 0.6$) and ($55 \text{ ke} \lesssim Q_\Sigma \lesssim 75 \text{ ke}$). They originate from single-photon energy depositions in the ground lead connecting to the

absorber. This lead is attached asymmetrically to the detector, very close to junction 1. Therefore, a fraction of the quasiparticles generated in the ground electrode leak into that STJ and contribute a measurable signal. This effect exemplifies that one can in principle design any absorber shape appropriate for a specific imaging purpose.

The expected number N_0 of excited quasiparticles generated upon deposition of energy E is $N_0 = E/1.7\Delta$ where Δ is the energy gap of the superconducting absorber and 1.7Δ is the effective energy to create one quasiparticle.^{19,20,21} Note that the energy conversion factor 1.7 is appropriate for Ta, but in general it is material dependent.²¹ The intrinsic energy fluctuations ε_i of STJs can be described in first order by²²

$$\varepsilon_i = \sqrt{1.7\Delta(F + 1 + \langle n \rangle^{-1})}, \quad (1)$$

where $F \approx 0.2$ is the Fano factor^{19,20}, and $\langle n \rangle$ is the average number each quasiparticle contributes to the charge signal due to backtunneling.² The energy-resolving power R is conventionally described by $R = E/2.355\varepsilon_i$ where the factor 2.355 scales between standard deviation and full width at half maximum of a normal distribution.

A. Linear response and spectral resolution

At temperatures well below the superconducting transition temperature, where quasiparticle recombination processes are very slow, and for sufficiently low energy densities of the nonequilibrium quasiparticle distribution (i.e. for optical photons, where self-recombination is negligible), a linear response of the detector is predicted for single STJ detectors²³ as well as for DROIDS.²⁴ In order to test the linearity of our detectors we performed measurements with photon energies ranging from IR to UV. Similar to Figs. 1(b) and (d) we consider only photon events with interactions in a narrow window of the absorber's central region, i.e. satisfying $|x_0| < 0.05$. In addition to single-photon events we also extract the signals due to simultaneous two-photon events where data of minimum interaction distance is selected. This condition corresponds to the low edge of the two-photon events contour in Fig. 1(a) and to the prominent peak at ~ 160 ke in Fig. 1(b), whereas events of two photons interacting at largest distance (i.e. close to the junctions) are expected to appear at the upper contour edge.

The results of detected total charge Q_Σ as a function of photon energy are shown in Fig. 2(a). Solid dots and open circles correspond to single and two photons, respectively. The horizontal error bars refer to the spectral widths ε_λ of the LEDs, the vertical errors reflect the measured distribution spreads q_m of signal amplitudes. A linear least-square fit to the data points yields

$$\eta \doteq Q_\Sigma/E = 23843 e/eV.$$

This is by a factor 28.4 times more charge output than the theoretically generated $N_0 = 840$ quasiparticles per eV in

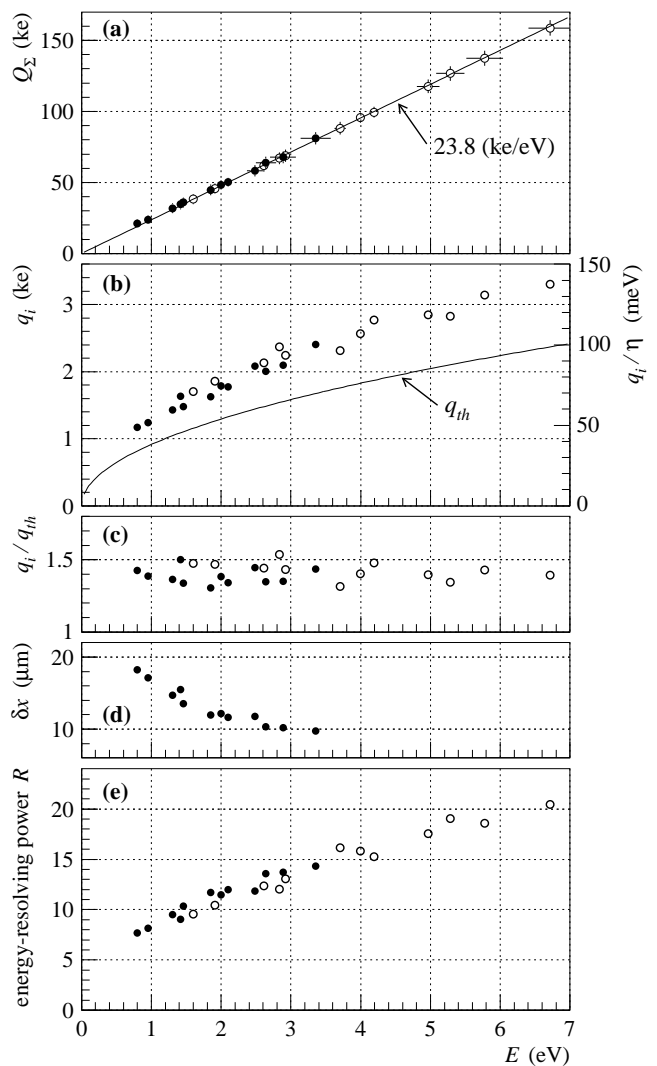


FIG. 2: (a) Detected total charge as a function of photon energy. Full dots and open circles correspond to single and two-photon events, respectively. The horizontal error bars are the specified spectral widths of the LEDs, the vertical errors are taken from the experimental detector signal distributions. The straight line is a least-square fit to the data points with a slope as indicated. (b) Intrinsic experimental detector noise (electronic noise and photon energy spread subtracted) versus energy. The drawn line is a theoretically predicted thermodynamic limit. The right ordinate relates the data to units of eV. (c) Ratio of measured to theoretical intrinsic detector noise. (d) Estimated onedimensional position resolution. (e) Energy-resolving power $R = Q_\Sigma/2.355q_i$.

a Ta absorber, where $\Delta_{\text{Ta}} = 0.7$ meV. This amplification is attributed to the device-internal gain due to backtunneling. In the case of lossless diffusion the responsivity would even amount to 27.9 ke/eV (see Sec. III B), corresponding to an average backtunneling factor $\langle n \rangle = 33.2$.

We found no significant deviations from linearity within experimental errors over the entire measured energy range including the data from two-photon events.

This is most remarkable because it proves not only the proportional regime considered in Refs. 23,24 but also an energy-independent backtunneling process at these quasiparticle densities.

By subtracting the readout electronics noise q_e and the spectral widths ε_λ of the LEDs from the measured pulse-height distribution spreads q_m we deduce the device-intrinsic charge fluctuations q_i as $q_i^2 = q_m^2 - q_e^2 - (\varepsilon_\lambda \eta)^2$. Figure 2(b) shows q_i as a function of energy together with the theoretical fluctuations $q_{th} = \varepsilon_\lambda \eta$ as given by Eq. (1). The ratio $q_i/q_{th} \approx 1.4$ plotted in Fig. 2(c) suggests that the performance of our detectors is close to the thermodynamic limit imposed by the simple model (1). The constant ratio implies that further additive, energy-independent terms in Eq. (1) may better account for the device-intrinsic fluctuations.^{25,26}

If we neglect quasiparticle losses during diffusion, the charge noise can be translated into an imaging position resolution $\delta x \approx (L_{Ta}/x_{max})(q_i/Q_\Sigma)$ as displayed in Fig. 2(d), where $x_{max} = 0.41$ in our devices accounts for the reduced trapping efficiency (see Sec. III B). The energy-dependent number of effective pixels $\sim L_{Ta}/2.355\delta x$ is in our case in the range of 3...6 (neglecting the real geometry where about one third of the absorber is modified by trapping regions). A possible improvement in position resolution, however, can be obtained for longer absorbers (for the price of reduced energy resolution due to diffusion losses) by measuring the time delay of the charge signals in the two channels. Assuming a moderate timing accuracy of $1\mu s$ we estimate from our timing measurements (roughly $6\mu s$ differential delay over $L_{b,Ta}$, see Sec. III B) a spatial resolution of ~ 6 pixels, which is already comparable to the charge-noise limited values.

Finally, the energy-resolving power R of our DROIDS is plotted in Fig. 2(e), showing a comfortable signal-to-noise ratio for single-photon imaging down to near IR wavelengths.

B. Quasiparticle diffusion

After localized energy deposition in a superconductor, cascades of several fast processes eventually end with a population of excess quasiparticles. Those initial conversion processes are negligibly fast compared to quasiparticle recombination and loss times.^{20,27} Therefore, we expect our measurable device dynamics to be dominated by diffusion and subsequent trapping and tunneling processes. Quasiparticle diffusion in the absorber can be described by the onedimensional equation

$$\frac{\partial}{\partial t}n(x,t) - D\frac{\partial^2}{\partial x^2}n(x,t) + \frac{1}{\tau_{loss}}n(x,t) = 0, \quad (2)$$

where $n(x,t)$ is the quasiparticle density, D is the diffusion constant, and τ_{loss}^{-1} is the loss rate in the Ta absorber. We adopt the phenomenological model in Ref. 6 which

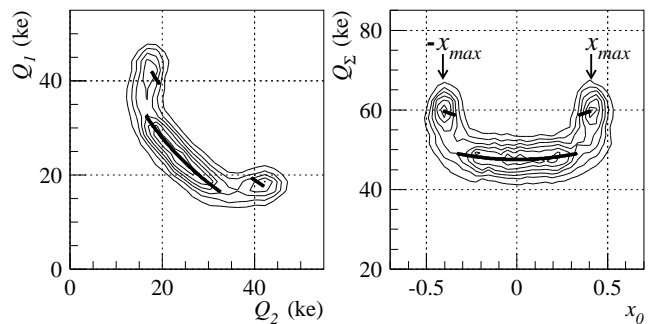


FIG. 3: Contour plots of a measurement with $\lambda = 592$ nm photons (only single-photon events are shown). The thick line represents the result of a model fitted to the data points, where we assume onedimensional quasiparticle diffusion with losses and a reduced gap in the trap region of the Ta absorber due to proximity of Al. Photon absorption in the trap region is identified with events at $x_0 = \pm x_{max}$.

derives the final integral of collected charges $Q_{k=1,2}$ at the two STJs

$$Q_k(x_0) = Q_0 \frac{\sinh \xi_k \alpha + \beta \cosh \xi_k \alpha}{(1 + \beta^2) \sinh \alpha + 2\beta \cosh \alpha}, \quad (3)$$

where $\xi_k = |x_0 - (-1)^k|/2$ is a normalized photon position relative to junction k , the dimensionless parameter $\alpha = L/\sqrt{D\tau_{loss}}$ measures the quasiparticle diffusion length $\Lambda = L/\alpha$ relative to the absorber length, and $\beta = (\tau_{trap}/\tau_{loss})^{1/2}$ compares the trapping rate τ_{trap}^{-1} to the loss rate.

This model allows us to fit the experimental data as shown in Fig. 3. In our specific devices, we have to distinguish between the bare Ta absorber and the proximized region due to trapping layers, where the effective gap energy relevant for quasiparticle generation is reduced. Those regions are separated at $|x_0| \approx 0.3$. The position identified with energy depositions directly in the trap region is $x_{max} = 0.41$ in our DROIDS. Because α accounts for the curvature (losses) and β for the given x_{max} (trapping), we can fit Eq. (3) to the data in the limited range $|x_0| < 0.3$, yielding the fit parameters $\alpha = 0.63$, $\beta = 0.57$ and $Q_{0,b} = 58.6$ ke for the bare absorber. Applying the same function to the data for $|x_0| > 0.3$ while keeping the formerly found α and β fixed yields $Q_{0,t} = 69.1$ ke in the trap regions. This implies that the mean gap energy in the trap region where quasiparticle generation takes place is reduced by $(1 - Q_{0,b}/Q_{0,t}) = 15.2\%$. The empirical fit to a Monte Carlo simulation¹⁴ has found a reduction of about 12.5% for the same devices. The discrepancy between the results from the two approaches is acceptable considering the uncertainties in empirical parameter adjustment in the latter method. One should note that the energy gap of $0.848\Delta_{Ta} = 594\mu eV$ in the trap region is not equivalent to the one at the tunnel barrier where about $450\mu eV$ was found from current-voltage characteristics measurements. This is well understood in terms of the superconducting proximity effect.²⁸

For the parameter β the simulations¹⁴ found $\beta \approx (P_{\text{loss,Abs}}/P_{\text{trap}})^{1/2} = 0.483$. This value is slightly lower than our model fit parameter because the simulations¹⁴ consider a trapping and a tunneling probability separately (i.e. a nonvanishing detrapping probability), whereas our model averages over trapping and detrapping processes and therefore results in a lower effective trapping rate.

The quasiparticle diffusion length in our absorber, i.e. the average length a quasiparticle travels before being lost by recombination or other loss channels, is

$$\Lambda = \frac{L_{\text{Ta}}}{\alpha} = 214 \mu\text{m},$$

which suggests that there is still room for a longitudinal extension of the absorber. In the expression above we use L_{Ta} (and not $L_{\text{b,Ta}}$) as the effective absorber length based on the following argument: A quasiparticle entering the trap region travels, if not tunneling before, a distance $2L_j$ until it has the first chance to detrap. The average trapping length $\Lambda\beta^2$ is on the order of $2L_j$ (calculated with either L_{Ta} or $L_{\text{b,Ta}}$). The mean distance in the trap region travelled by quasiparticles which are being trapped is therefore roughly L_j . Consequently, the absorber length relevant for our analysis is $L_{\text{b,Ta}} + 2L_j = L_{\text{Ta}}$. Alternatively, we can consider quasiparticles starting in the trap region with arbitrary direction and position. Those which are detected in the opposite STJ travel in average a distance L_j before leaving the trap. Therefore, the events at $|x_{\text{max}}|$ in Fig. 3 are identified with the physical positions at $\pm L_{\text{Ta}}/2$, and not with the edge of the transition from bare absorber to trap region at $\pm L_{\text{b,Ta}}/2$.

Measurements of the trigger time differences δt_m between the two pulse-shaped detector signals for thresholds set arbitrarily at 33% and 67% of the peak amplitudes are shown in Fig. 4. An S-shaped timing versus position curve, which we observed for fast signals, was stretched to a straight line after pulse-shaping with a time constant one order of magnitude larger than the original signal rise-time. The results of a linear fit to the data points in the range $|x_0| < 0.3$ are included in the figure. The events corresponding to photon hits in the trap regions are excluded from the fit because they show a slight extra time delay.

This observation is interpreted as a consequence of delayed detrapping, namely the quasiparticles detected in the opposite STJ have a non-zero probability to propagate within the trap for some time before leaving for the other side. In addition, they may initially go through a few backtunneling cycles, which further delays the opposite charge signal by the extra tunneling times.

We have numerically simulated the quasiparticle propagation according to Eq. (2) to determine the detector-signal dynamics including the response of readout electronics and pulse shaping. The normalized timing differences δt_n between the two channels calculated for trigger thresholds at 33% and 67% were 0.336 and 0.351, respectively, assuming $D = L = 1$. Scaling the measured

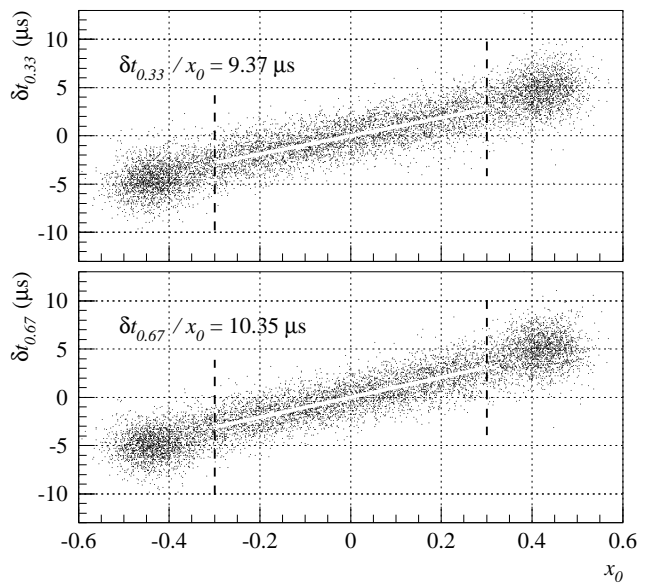


FIG. 4: Measured time differences between the two detector channels versus position, for trigger thresholds at 33% (top) and at 67% (bottom) of the signal peak amplitudes. The white lines are linear fits to the data in the range $|x_0| < 0.3$. The resulting fit parameter is included in the plots.

data with these results allows us to estimate the diffusion constant

$$D \approx \frac{\delta t_n}{2\delta t_m x_{\text{max}}} L_{\text{Ta}}^2 \approx 7.8 \frac{\text{cm}^2}{\text{s}}.$$

For comparison, a theoretically evaluated diffusion constant is given by²⁹

$$D_{\text{th}} = \sqrt{\frac{k_B T}{2\pi\Delta}} v_F^2 \tau_{\text{imp}},$$

where $v_F = 1.6 \times 10^8 \text{cm}^2\text{s}^{-1}$ is the Fermi velocity of electrons in the superconductor, $\tau_{\text{imp}} = m_e/\rho_{\text{LT}} n e^2$ is the impurity-scattering time, m_e is the electron rest mass and $n = 5.52 \times 10^{22} \text{cm}^{-3}$ the density of conduction electrons in Ta.³⁰ With $\rho_{\text{LT}} = 0.5 \times 10^{-8} \Omega\text{m}$ (or $\rho_{\text{RT}} = 13 \times 10^{-8} \Omega\text{m}$ and $RRR = 25$, respectively) and at $T = 310 \text{mK}$ we obtain $D_{\text{th}} = 25.2 \text{cm}^2\text{s}^{-1}$, which is more than three times the experimentally determined value. Similar discrepancies between experiment and theoretical predictions were systematically observed in other experiments^{7,8,10,11,30,31} and remain unresolved.

The quasiparticle loss time deduced from the measurements is found to be $\tau_{\text{loss}} = \Lambda^2 D^{-1} \approx 58.9 \mu\text{s}$, which is significantly longer than the tunneling time of about $1 \mu\text{s}$. However, the trapping process with a time constant $\tau_{\text{trap}} = \beta^2 \tau_{\text{loss}} \approx 18.9 \mu\text{s}$ should preferably be improved in our devices towards faster trapping rates, in order to enhance $x_{\text{max}} \rightarrow 1$ for better position resolution.

Alternatively to our phenomenological discussion on imaging resolution in the previous section, the resolving

capabilities have been derived analytically²⁴ with a prediction for

$$\delta x \approx \sqrt{D\tau_{\text{loss}}} \frac{q_i}{Q_\sigma} = \Lambda \frac{q_i}{Q_\sigma}.$$

Inserting our experimental results (always for single-photon events only) yields position resolutions in the range $\delta x \approx 26.7 \dots 14.8 \mu\text{m}$, corresponding to $5 \dots 9$ pixels for our detector. This is in fair agreement with our former approximations. However, we wish to emphasize that all these rough estimates ignore the geometrical properties of the real absorber, which needs to be taken into account for a quantitatively precise analysis of position resolution.³²

IV. CONCLUSIONS

Detection of single (and simultaneous multiple) photons with good spectral and spacial resolution was performed with STJ based DROIDS. Single-photon resolution down to near IR energies was proven, with a perfectly linear energy response over the entire UV to IR wavelength range. Sensitivity to the investigated photon energies was possible due to the backtunneling effect, delivering in our case a device-intrinsic gain of about 33, which is a feature unique to STJs. The detectors were found to operate close to the thermodynamic limit imposed by particle fluctuation statistics.

The measured dynamic response of the DROIDS was compared to numerical modelling based on quasiparticle

diffusion including loss and trapping processes. The parameters extracted from experimental data are physically meaningful and coincide reasonably with former Monte Carlo simulations.¹⁴ However, the diffusion constant was found to significantly disagree with theoretical predictions, similar to all preceding experiments of the same kind.

Position resolution of our relatively short absorber was estimated to about $3 \dots 6$ equivalent pixels for photon energies in the range $0.8 \dots 3.4 \text{ eV}$. By taking the differential time delays of the two channels into account, we predict an improvement in position resolution by at least a factor of two for a longer absorber ($L_{\text{Ta}} \rightarrow \Lambda$) and better trapping efficiencies ($\tau_{\text{trap}} \ll \tau_{\text{loss}}$).

High-sensitivity spectrometers with single-photon counting capabilities in the broad optical range are not only of high interest for astronomical observations. Single photons at the telecommunication wavelength of 1550 nm are currently used, e.g., in intense studies on quantum cryptography,³³ which links information theory to quantum entanglement physics. Hence, STJ based DROIDS with the properties and potential as presented in this paper may as well be an interesting and natural choice for IR single-photon counting experiments.

Acknowledgments

We are grateful to Elmar Schmid for ceaseless improvement of the readout electronics, to Iwan Jerjen and Philippe Lerch for valuable discussions and experimental assistance, and to Fritz Burri for technical support.

-
- ¹ N. E. Booth and D. J. Goldie, *Supercond. Sci. Technol.* **9**, 493 (1996).
- ² K. E. Gray, *Appl. Phys. Lett.* **32**, 392 (1978).
- ³ M. A. C. Perryman, M. Cropper, G. Ramsay, F. Favata, A. Peacock, N. Rando, and A. Reynolds, *Mon. Not. R. Astron. Soc.* **324**, 899 (2001).
- ⁴ D. D. E. Martin, P. Verhoeve, A. Peacock, A. van Dordrecht, J. Verveer, and R. Hijmering, *Nucl. Instrum. Methods Phys. Res. A* **520**, 512 (2004).
- ⁵ H. Kraus, F. von Feilitzsch, J. Jochum, R. L. Mössbauer, Th. Peterreins, and F. Pröbst, *Phys. Lett. B* **231**, 195 (1989).
- ⁶ J. Jochum, H. Kraus, M. Gutsche, B. Kemmather, F. v. Feilitzsch, and R. L. Mössbauer, *Ann. Physik* **2**, 611 (1993).
- ⁷ S. Friedrich, K. Segall, M. C. Gaidis, C. M. Wilson, D. E. Prober, A. E. Szymkowiak, and S. H. Moseley, *Appl. Phys. Lett.* **71**, 3901 (1997).
- ⁸ E. C. Kirk, Ph. Lerch, J. Olsen, A. Zehnder, and H. R. Ott, *Nucl. Instrum. Methods Phys. Res. A* **444**, 201 (2000).
- ⁹ L. Li, L. Frunzio, K. Segall, C. M. Wilson, D. E. Prober, A. E. Szymkowiak, and S. H. Moseley, *Nucl. Instrum. Methods Phys. Res. A* **444**, 228 (2000).
- ¹⁰ R. den Hartog, D. Martin, A. Kozorezov, P. Verhoeve, N. Rando, A. Peacock, G. Brammert, M. Krumrey, D. J. Goldie, and R. Venn, *Proc. SPIE* **4012**, 237 (2000).
- ¹¹ L. Li, L. Frunzio, C. M. Wilson, and D. E. Prober, *J. Appl. Phys.* **93**, 1137 (2003).
- ¹² C. M. Wilson, K. Segall, L. Frunzio, L. Li, D. E. Prober, D. Schiminovich, B. Mazin, C. Martin, and R. Vasquez, *Nucl. Instrum. Methods Phys. Res. A* **444**, 449 (2000).
- ¹³ P. Verhoeve, R. den Hartog, D. Martin, N. Rando, A. Peacock, and D. J. Goldie, *Proc. SPIE* **4008**, 683 (2000).
- ¹⁴ I. Jerjen, E. Kirk, E. Schmid, and A. Zehnder, *Nucl. Instrum. Methods Phys. Res. A* **559**, 497 (2006).
- ¹⁵ R. A. Hijmering, P. Verhoeve, D. D. E. Martin, A. Peacock, and A. G. Kozorezov, *Nucl. Instrum. Methods Phys. Res. A* **559**, 689 (2006).
- ¹⁶ R. A. Hijmering, P. Verhoeve, D. D. E. Martin, A. Peacock, A. G. Kozorezov, and R. Venn, *Nucl. Instrum. Methods Phys. Res. A* **559**, 692 (2006).
- ¹⁷ J. H. Weaver, D. W. Lynch, and C. G. Olson, *Phys. Rev. B* **10**, 501 (1974).
- ¹⁸ F. Gervais, in *Handbook of optical constants of solids II*, edited by E. D. Palik (Academic, San Diego, CA, 1991), p. 761.
- ¹⁹ M. Kurakado, *Nucl. Instrum. Meth.* **196**, 275 (1982).
- ²⁰ N. Rando, A. Peacock, A. van Dordrecht, C. Foden, R. Engelhardt, B. G. Taylor, P. Gare, J. Lumley, and C. Pereira, *Nucl. Instrum. Methods Phys. Res. A* **313**, 173 (1992).

- ²¹ A. Zehnder, Phys. Rev. B **52**, 12858 (1995).
- ²² D. J. Goldie, P. L. Brink, C. Patel, N. E. Booth, and G. L. Salmon, Appl. Phys. Lett. **64**, 3169 (1994).
- ²³ B. Ivlev, G. Pepe, and U. Scotti di Uccio, Nucl. Instrum. Methods Phys. Res. A **300**, 127 (1991).
- ²⁴ E. Esposito, B. Ivlev, G. Pepe, and U. Scotti di Uccio, J. Appl. Phys. **76**, 1291 (1994).
- ²⁵ K. Segall, C. Wilson, L. Frunzio, L. Li, S. Friedrich, M. C. Gaidis, D. E. Prober, A. E. Szymkowiak, and S. H. Moseley, Appl. Phys. Lett. **76**, 3998 (2000).
- ²⁶ D. D. E. Martin, P. Verhoeve, A. Peacock, A. G. Kozorezov, J. K. Wigmore, H. Rogalla, and R. Venn, Appl. Phys. Lett. **88**, 123510 (2006).
- ²⁷ A. G. Kozorezov, A. F. Volkov, J. K. Wigmore, A. Peacock, A. Poelaert, and R. den Hartog, Phys. Rev. B **61**, 11807 (2000).
- ²⁸ A. Zehnder, Ph. Lerch, S. P. Zhao, Th. Nussbaumer, E. C. Kirk, and H. R. Ott, Phys. Rev. B **59**, 8875 (1999).
- ²⁹ V. Narayanamurti, R. C. Dynes, P. Hu, H. Smith, and W. F. Brinkman, Phys. Rev. B **18**, 6041 (1978).
- ³⁰ Th. Nussbaumer, Ph. Lerch, E. Kirk, A. Zehnder, R. Füchslin, P. F. Meier, and H. R. Ott, Phys. Rev. B **61**, 9719 (2000).
- ³¹ K. Segall, C. Wilson, L. Li, L. Frunzio, S. Friedrich, M. C. Gaidis, and D. E. Prober, Phys. Rev. B **70**, 214520 (2004).
- ³² M. Ejrnaes, C. Nappi, and R. Cristiano, Supercond. Sci. Technol. **18**, 953 (2005).
- ³³ N. Gisin, G. Ribordy, W. Tittel, and H. Zbinden, Rev. Mod. Phys. **74**, 145 (2002).